

On the Possibility of Tuning Molecular Edges To Direct Supramolecular Self-Assembly in Coumarin Derivatives through Cooperative Weak Forces: Crystallographic and Hirshfeld Surface Analyses

Saikat Kumar Seth,^{†,§} Debayan Sarkar,[‡] Atish Dipankar Jana,^{*,#} and Tanusree Kar^{*,†}

[†]Department of Materials Science, Indian Association for the Cultivation of Science, Jadavpur, Kolkata 700 032, India

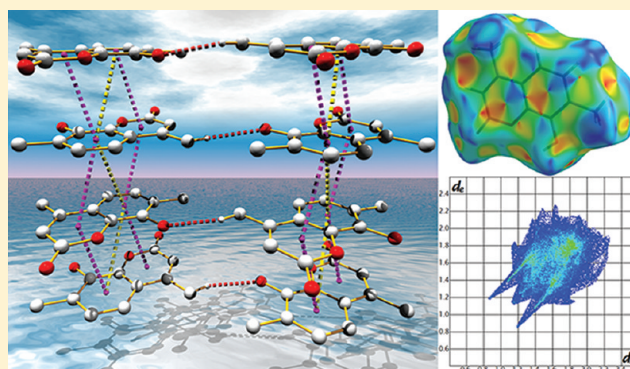
[§]Department of Physics, M. G. Mahavidyalaya, Bhupatinagar, Midnapore (East), West Bengal 721 425, India

[‡]Department of Chemistry, A. B. N. Seal College, Coochbehar 736101, W.B., India

[#]Department of Physics, Behala College, Parnasree, Kolkata-700060, India

S Supporting Information

ABSTRACT: Four organic compounds based on substituted coumarin derivatives (1–4) have been synthesized and characterized by X-ray structural studies with a detailed analysis of Hirshfeld surface and fingerprint plots facilitating a comparison of intermolecular interactions in building different supramolecular architectures. The X-ray study reveals that in the molecular packing C–H···O, π ··· π , and carbonyl (lone pair)··· π interactions cooperatively take part. The recurring feature of the self-assembly in all the compounds is the appearance of the molecular ribbon through weak hydrogen bonding. These hydrogen bonded ribbons further stacked into molecular layers by π ··· π forces. The mode of cooperativity of the weak C–H···O and π ··· π forces is such that they operate in mutually perpendicular directions — hydrogen bonding in the plane of the molecule at their edges and π -stacking perpendicular to the molecular plane. Investigation of intermolecular interactions and crystal packing via Hirshfeld surface analyses reveals that more than two-thirds of the close contacts are associated with weak interactions. Hirshfeld surface and breakdown of the corresponding fingerprint plots of four coumarin structures clearly quantify the interactions within the crystal structures, revealing significant similarities in the interactions experienced by each compound. The binding energies associated with the weak interactions have been estimated using density functional theory calculations.



INTRODUCTION

Molecular self-assembly through weak noncovalent forces is the hallmark of biological systems. An understanding of mutual influence of more than one noncovalent force in the self-assembly of molecules and ions is the key in successful utilization of these forces in various branches of science such as crystal engineering,¹ host–guest chemistry,² supramolecular electronics³ and nanoscale technology,⁴ etc. Among a number of noncovalent forces such as hydrogen bonding,⁵ π ··· π ,⁶ C–H··· π ,⁷ cation··· π ,⁸ anion··· π ,⁹ lone-pair··· π ,¹⁰ S···S,¹¹ Se···Se,¹² and various metal···metal interactions,¹³ hydrogen bonding interaction, and π ··· π interaction have been widely utilized in directing molecular assembly for the construction of various supramolecular architectures. Proper organization of complementary donor and acceptor atoms on the molecule is essential in utilizing hydrogen bond to direct molecular self-assembly.

Substituted coumarin molecules are simple systems that have been extensively studied in the context of solid state photochemical

reactivity,¹⁴ that is, [2 + 2] photocycloaddition, and these are the molecules long-known for their pharmacological importance.¹⁵ These molecules possess molecular backbones capable of edge-to-edge self-association through weak but multiple C–H···O hydrogen bonds. Also as these molecules possess two fused aromatic rings, it is a common feature that molecular packing in a direction perpendicular to the molecular plane is governed by π -stacking interactions. Molecular assembly in these systems is the result of mutual cooperation between hydrogen bonding forces and π ··· π forces. Herein, we demonstrate how coumarin molecules may serve as remarkable skeletons for studying the pattern of self-association via complementary sites of multiple weak bonding such as hydrogen bonding and π ··· π interactions. The study of X-ray crystal structure of four coumarin based

Received: May 19, 2011

Revised: September 11, 2011

Published: September 22, 2011

Table 1. Crystal Data and Structure Refinement Parameters for Compounds C₁₁H₁₀O₂ (1), C₁₁H₁₀O₃ (2), C₁₁H₁₀O₃ (3), and C₁₂H₁₀O₃ (4)^a

	compound (1)	compound (2)	compound (3)	compound (4)
formula weight	174.19	190.19	190.19	202.20
temperature	150(2) K	150 (2) K	150 (2) K	150(2) K
wavelength (Mo K α)	0.71073 Å	0.71073 Å	0.71073 Å	0.71073 Å
crystal system space group	triclinic $P\bar{1}$	monoclinic $P2_1/c$	monoclinic $C2/c$	monoclinic $P2_1/c$
unit cell parameters	$a = 7.0118(13)$ Å $b = 7.3848(17)$ Å $c = 9.9023(17)$ Å $\alpha = 95.805(2)^\circ$ $\beta = 106.502(3)^\circ$ $\gamma = 110.677(2)^\circ$	$a = 7.038(1)$ Å $b = 9.396(3)$ Å $c = 13.358(1)$ Å $\alpha = 90.00^\circ$ $\beta = 98.932(6)^\circ$ $\gamma = 90.00^\circ$	$a = 12.529(8)$ Å $b = 12.889(3)$ Å $c = 12.689(4)$ Å $\alpha = 90.00^\circ$ $\beta = 115.679(2)^\circ$ $\gamma = 90.00^\circ$	$a = 4.1622(5)$ Å $b = 10.589(1)$ Å $c = 21.932(3)$ Å $\alpha = 90.00^\circ$ $\beta = 91.696(4)^\circ$ $\gamma = 90.00^\circ$
volume	448.21(15) Å ³	872.6(3) Å ³	1846.7(14) Å ³	966.2(2) Å ³
Z, calculated density	2, 1.291 Mg/m ³	4, 1.448 Mg/m ³	8, 1.368 Mg/m ³	4, 1.390 Mg/m ³
absorption coeff	0.088 mm ⁻¹	0.106 mm ⁻¹	0.100 mm ⁻¹	0.100 mm ⁻¹
F(000)	184	400	800	424
crystal size	0.21 × 0.13 × 0.08 mm	0.19 × 0.12 × 0.07 mm	0.25 × 0.16 × 0.09 mm	0.21 × 0.18 × 0.13 mm
θ -range for data collection	2.20–25.00°	2.66–25.00°	2.40–24.98°	1.86–24.99°
limiting indices	$-8 \leq h \leq 7$ $-8 \leq k \leq 8$ $-11 \leq l \leq 11$	$-8 \leq h \leq 8$ $-11 \leq k \leq 11$ $-15 \leq l \leq 15$	$-14 \leq h \leq 14$ $-15 \leq k \leq 15$ $-15 \leq l \leq 14$	$-4 \leq h \leq 4$ $-12 \leq k \leq 12$ $-26 \leq l \leq 26$
reflections collected/unique completeness to θ (%)	3240/1563 [R(int) = 0.0138] 98.8	7715/1536 [R(int) = 0.0273] 99.9	8466/1626 [R(int) = 0.0331] 100	8738/1692 [R(int) = 0.0353] 100.0
refinement method	full-matrix least-squares on F^2	full-matrix least-squares on F^2	Full-matrix least-squares on F^2	Full-matrix least-squares on F^2
data/restraints/parameters	1563/0/120	1536/0/131	1626/0/129	1692/0/136
goodness-of-fit on F^2	1.066	1.066	1.044	1.069
final R indices [$I > 2\sigma(I)$]	$R_1 = 0.0424$, $wR_2 = 0.1160$	$R_1 = 0.0333$, $wR_2 = 0.0945$	$R_1 = 0.0444$, $wR_2 = 0.1221$	$R_1 = 0.0365$, $wR_2 = 0.0898$
R indices (all data)	$R_1 = 0.0552$, $wR_2 = 0.1273$	$R_1 = 0.0345$, $wR_2 = 0.0962$	$R_1 = 0.0597$, $wR_2 = 0.1363$	$R_1 = 0.0473$, $wR_2 = 0.0970$
largest diff peak and hole	0.133 and -0.170 e \cdot Å ⁻³	0.188 and -0.224 e \cdot Å ⁻³	0.159 and -0.228 e \cdot Å ⁻³	0.139 and -0.246 e \cdot Å ⁻³

^a $R_1 = \sum ||F_o| - |F_c|| / \sum |F_o|$, $wR_2 = [\sum \{ (F_o^2 - F_c^2)^2 \} / \sum \{ w(F_o^2)^2 \}]^{1/2}$, $w = 1 / \{ \sigma^2(F_o^2) + (aP)^2 + bP \}$, where $a = 0.0618$ and $b = 0.0549$ for 1; $a = 0.0552$ and $b = 0.2771$ for 2; $a = 0.0834$ and $b = 0.2841$ for 3; and $a = 0.0448$ and $b = 0.2312$ for 4. $P = (F_o^2 + 2F_c^2) / 3$ for all the title structures.

compounds reveals that hydrogen bonding and $\pi \cdots \pi$ forces operate in a particular mutually cooperative fashion. This study also indicates the possibility of engineering the molecular edges of the coumarin framework to obtain various coumarin based self-assembled molecular architectures. The Hirshfeld surface analysis and associated fingerprint plots have been presented to explore the nature of intermolecular interactions in the title crystal structures and offering considerable potential in the context of crystal engineering.

EXPERIMENTAL SECTION

Materials and Measurements. All chemicals were of analytical grade and used without further purification. Elemental analyses (C, H, and N) were performed on a Perkin-Elmer 2400 elemental analyzer. IR spectra were recorded on a Perkin-Elmer L120-00 FT-IR spectrophotometer with the sample prepared as a KBr pellet. All NMR spectra were recorded at 300 K on a Bruker DRX-300 spectrometer operating at the frequencies of 300.0 MHz (¹H), 75.0 MHz (¹³C). The spectra were measured in CDCl₃ solution and the sample concentrations ranged from 40 to 70 mg per 0.4 mL of solvent, in a 5 mm sample tube.

Preparation of Compound 1 (Literature Known).¹⁶ To a well stirred solution of 8 mL of concentrated H₂SO₄ at 100 °C, a mixture of m-cresol (10 g, 0.09 mol) and ethyl acetoacetate (17.01 g, 0.135 mol) was added and stirred for 3 h. Then the reaction mixture was cooled and

ice-cold water was added. A yellow solid separated out which was filtered, dried, and crystallized from methanol to yield 8 g (0.045 mol) of 1 in 51% yield as colorless plates. m.p. 154 °C; IR (KBr) ν^{\max} 1687 cm⁻¹. ¹H NMR (500 MHz, CDCl₃) δ 7.3 (d, $J = 8.2$ Hz, 1H); 6.8 (d, $J = 8.2$ Hz, 1H), 6.7 (s, 1H); 6.4 (s, 1H); 2.4 (s, 3H); 2.35 (s, 3H). ¹³C NMR (125 MHz, CDCl₃) δ 157.8, 150.2, 149.8, 135.6, 123.4, 122.8, 114.8, 113.7, 111.3, 23.6, 19.6. HRMS (EI) C₁₁H₁₀O₂. MH⁺ Found: 175.0578, calculated: 175.0579. Anal. Calcd. for C₁₁H₁₀O₂: C, 75.87; H, 5.74. Found: C, 75.90; H, 5.71.

Preparation of Compound 2. To a well stirred solution of 8 mL of concentrated H₂SO₄ at 100 °C, a mixture of 3-methyl benzene 1, 2 diol (10 g, 0.0526 mol) and ethyl acetoacetate (10 g, 0.0789 mol) was added and stirred for 3 h. Then the reaction mixture was cooled and ice-cold water was added. A brown colored solid separated out which was filtered, dried, and crystallized from ethanol to yield 6.2 g (0.0326 mol) of 2 in 62% yield light brown crystals. m.p. 162 °C; IR (KBr) ν^{\max} 3321, 1690 cm⁻¹. ¹H NMR (500 MHz, CDCl₃) δ 7.6 (d, $J = 8.2$ Hz, 1H); 6.9 (d, $J = 8.2$ Hz, 1H); 6.6 (s, 1H); 5.5 (brs, 1H); 2.5 (s, 3H); 2.2 (s, 3H). ¹³C NMR (125 MHz, CDCl₃) δ 159.8, 148.3, 147.8, 139.8, 128.4, 123.2, 118.8, 117.2, 112.6, 20.6, 17.3. HRMS (EI) C₁₁H₁₀O₃. MH⁺ Found: 191.0531, calculated: 191.0528. Anal. Calcd. for C₁₁H₁₀O₃: C, 69.46; H, 5.30. Found: C, 69.48; H, 5.32.

Preparation of Compound 3. A solution of 6-hydroxy-7-methylcoumarin (1.52 g, 8.52 mol), anhydrous potassium carbonate (1.4 g, 10.14 mol), and methyl iodide (1.7 g, 11.9 mol) in acetone (20 mL) was

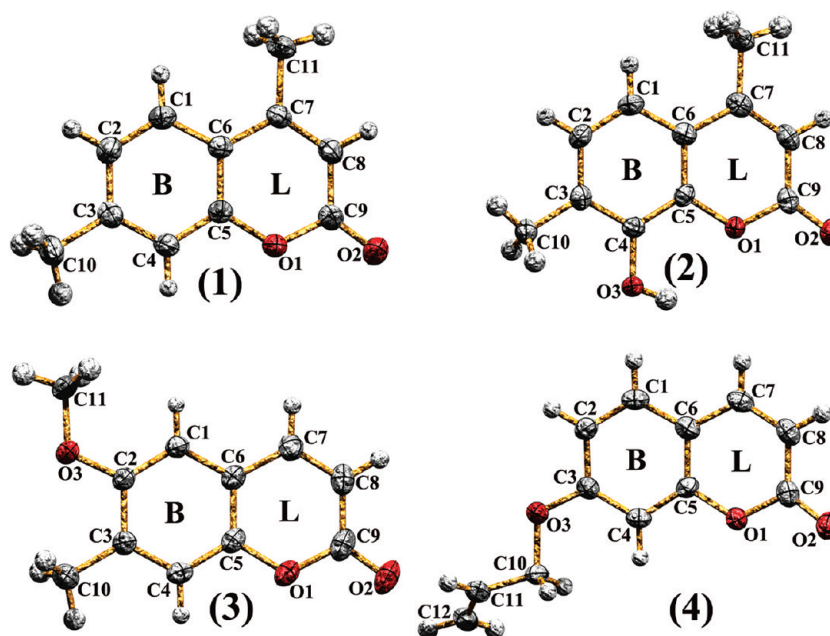


Figure 1. ORTEP view (granite stone) with atom numbering scheme of compounds 1–4 with displacement ellipsoids at the 30% probability level.

refluxed for 8 h. The reaction mixture was cooled and most of the acetone was distilled off. The residue was poured into water and extracted with chloroform (3×30 mL). The combined organic extract was washed with water, dried, and concentrated to afford a yellow solid, which was crystallized from ethanol to furnish 6-methoxy-7-methylcoumarin **3** (1.33 g, 82%) as a yellowish crystal. m.p. $132\text{--}134$ °C. IR (KBr) ν^{max} 1716 cm^{-1} . $^1\text{H NMR}$ (300 MHz, CDCl_3) δ 7.65 (d, $J = 9.5$ Hz, 1H); 7.12 (s, 1H); 6.79 (s, 1H); 6.36 (d, $J = 9.5$ Hz, 1H); 3.87 (s, 3H); 2.30 (s, 3H). $^{13}\text{C NMR}$ (75 MHz, CDCl_3) δ 161.2, 154.4, 143.1, 132.6, 120.7, 118.4, 116.2, 115.4, 106.4, 55.6, 16.6. Anal. Calcd. for $\text{C}_{11}\text{H}_{10}\text{O}_3$: C, 69.46; H, 5.30. Found: C, 69.43; H, 5.29.

Preparation of Compound 4. A solution of 7-hydroxy-2H-chromen-2-one (1.5 g, 0.007 mol), anhydrous potassium carbonate (1.02 g, 0.007 mol), and allyl bromide (0.8 g, 0.007 mol) in acetone (20 mL) was refluxed for 10 h. The reaction mixture was cooled and most of the acetone was distilled off. The residue was poured into water and extracted with chloroform (3×30 mL). The combined organic extract was washed with water, dried, and concentrated to afford a colorless solid, which was crystallized from ethanol to furnish 7-(allyloxy)-2H-chromen-2-one **4** 1.18 g (0.005 mol, 84%) as a white crystals. m.p. $59\text{--}60$ °C. IR (KBr) ν^{max} 1720 cm^{-1} . $^1\text{H NMR}$ (300 MHz, CDCl_3) δ 7.7 (d, $J = 9.5$ Hz, 1H); 7.6 (d, $J = 8.2$ Hz, 1H); 6.8 (s, 1H); 6.2 (m, 1H); 5.97 (d, $J = 9.5$ Hz, 1H); 5.11 (d, $J = 14$ Hz, 1H); 4.98 (d, $J = 3$ Hz, 1H); 4.68 (s, 3H). $^{13}\text{C NMR}$ (75 MHz, CDCl_3) δ 159.05, 150.2, 145.7, 132.9, 130.5, 123.5, 112.7, 109.2, 108.3, 107.6, 100.6, 66.2. Anal. Calcd. for $\text{C}_{12}\text{H}_{10}\text{O}_3$: C, 71.28; H, 4.98. Found: C, 71.24; H, 4.96.

X-ray Crystallography Study. X-ray diffraction intensity data of the title compounds were collected at 150(2) K using a Bruker APEX-II CCD diffractometer. Data reduction was carried out using the program Bruker SAINT.¹⁷ The structure of the title compounds were solved by direct method and refined by the full-matrix least-squares technique on F^2 using the programs SHELXS97¹⁸ and SHELXL97,¹⁹ respectively. All the calculations were carried out using PLATON²⁰ and WinGX system Ver-1.64.²¹ All hydrogen atoms of the substituent groups were located from difference Fourier map and refined isotropically whereas all the hydrogen atoms attached to the ring carbons were placed at their geometrically idealized positions. A summary of crystal data and relevant

refinement parameters are given in Table 1. CCDC 819048–819050 (1–3) and 777025 (4) contain the supplementary crystallographic data for this paper. These data can be obtained free of charge from the Cambridge Crystallographic Data Centre via www.ccdc.cam.ac.uk/data_request/cif.

Computational Methods. For understanding the stability of various hydrogen bonded and π -stacking motifs some calculations were carried out. All calculations were performed using the PC GAMESS package.²² Initial geometries of the π -stacked dimers as well as hydrogen bonded dimers (trimer in one case) of substituted coumarin derivatives were taken from respective crystal structures. Starting from these initial geometries all dimeric and trimeric motifs were optimized to their minimum energy configurations. All calculations were performed at the density functional theory (DFT) level using X3LYP functional and 6-311++G** basis set. The stabilization energies of the n -meric (dimeric [$n = 2$] and trimeric [$n = 3$]) motifs involving n number of coumarin based molecules ($\Delta E_{n\text{-mer}}$) is calculated from the formula $\Delta E_{n\text{-mer}} = E_{n\text{-mer}} - (n \times E_{\text{monomer}})$. E_{monomer} was calculated by optimizing a single molecule at the same level of theory.

Hirshfeld Surface Analysis. Molecular Hirshfeld surfaces^{23–25,10p} in the crystal structure are constructed based on the electron distribution calculated as the sum of spherical atom electron densities.²⁶ For a given crystal structure and set of spherical atomic electron densities, the Hirshfeld surface is unique.²⁷ The normalized contact distance (d_{norm}) based on both d_e and d_i and the vdW radii of the atom, given by eq 1 enables identification of the regions of particular importance to intermolecular interactions.²³ The combination of d_e and d_i in the form of a two-dimensional (2D) fingerprint plot²⁸ provides a summary of intermolecular contacts in the crystal.²³ The Hirshfeld surfaces are mapped with d_{norm} and 2D fingerprint plots presented in this paper were generated using CrystalExplorer 2.1.²⁹ In CrystalExplorer, the internal consistency is important when comparing one structure with another; for the generation of Hirshfeld surfaces all bond lengths to hydrogen (or deuterium) atoms are set to typical neutron values (C–H = 1.083 Å, O–H = 0.983 Å, N–H = 1.009 Å).³⁰ Graphical plots of the molecular Hirshfeld surfaces mapped with d_{norm} used a red–white–blue color scheme, where red highlights shorter contacts, white is used for contacts around the vdW separation, and blue is for longer contacts. Moreover, two further colored

Table 2. Selected Bond Lengths (Å) and Bond Angles (°) for C₁₁H₁₀O₂ (1), C₁₁H₁₀O₃ (2), C₁₁H₁₀O₃ (3), and C₁₂H₁₀O₃ (4)

	compound (1)		compound (2)		compound (3)		compound (4)		mogul (mean)
	X-ray	DFT	X-ray	DFT	X-ray	DFT	X-ray	DFT	
Bond Lengths									
O1–C5	1.375(2)	1.351	1.380(1)	1.366	1.379(2)	1.357	1.381(2)	1.350	1.382
O1–C9	1.374(2)	1.353	1.375(1)	1.340	1.374(2)	1.350	1.384(2)	1.358	1.378
O2–C9	1.205(2)	1.185	1.213(1)	1.198	1.206(2)	1.185	1.215(2)	1.184	1.205
C8–C9	1.433(2)	1.462	1.444(2)	1.455	1.434(3)	1.468	1.444(2)	1.464	1.440
C7–C8	1.334(2)	1.335	1.348(2)	1.336	1.334(2)	1.331	1.342(2)	1.332	1.347
C6–C7	1.445(2)	1.464	1.450(2)	1.463	1.422(2)	1.452	1.433(2)	1.447	1.448
C5–C6	1.395(2)	1.387	1.393(2)	1.388	1.385(2)	1.376	1.390(2)	1.384	1.396
C7–C11	1.501(2)	1.504	1.496(2)	1.504					1.501
C3–C10	1.507(2)	1.509	1.503(2)	1.507	1.498(2)	1.507			1.510
C4–O3			1.359(2)	1.335					1.363
C2–O3					1.363(2)	1.351			1.367
C11–O3					1.429(2)	1.399			1.422
C3–O3							1.364(2)	1.339	1.372
C10–O3							1.445(2)	1.411	1.435
Bond Angles									
O1–C9–C8	117.14(14)	116.39	117.44(10)	117.30	117.20(15)	116.29	117.16(13)	116.27	117.06
O1–C5–C6	121.21(13)	121.66	122.03(10)	121.58	120.95(16)	121.65	120.71(12)	121.12	121.51
O1–C9–O2	116.28(15)	118.71	116.70(10)	118.37	116.69(19)	119.09	116.19(13)	118.44	116.33
C5–O1–C9	121.43(12)	123.17	120.97(9)	122.71	121.55(14)	123.39	122.00(11)	123.77	121.86
O2–C9–C8	126.57(15)	124.90	125.86(10)	124.32	126.1(2)	124.62	126.64(14)	125.29	125.94
C9–C8–C7	123.24(15)	122.49	122.69(10)	122.11	121.65(18)	121.21	121.13(14)	120.83	123.03
C2–C3–C4	118.26(15)	118.74	118.55(10)	118.94	118.64(15)	118.84	121.10(13)	120.36	117.98
C3–C4–C5	120.37(14)	120.09	119.51(10)	119.04	120.45(14)	120.53	117.58(13)	118.55	119.94
C2–O3–C11					117.13(14)	119.77			117.59
C3–O3–C10							116.78(11)	120.33	117.89

properties (shape index and curvedness) based on the local curvature of the surface can be specified.³¹

$$d_{\text{norm}} = \frac{d_i - r_i^{\text{vdw}}}{r_i^{\text{vdw}}} + \frac{d_e - r_e^{\text{vdw}}}{r_e^{\text{vdw}}} \quad (1)$$

RESULTS AND DISCUSSION

Structural Description. The molecular views (ORTEP)³² of the title coumarin derivatives **1–4** with atom numbering scheme is shown in Figure 1. X-ray crystal structure reveals the presence of a single coumarin molecule in the asymmetric unit of all compounds. The asymmetric units of the title compounds are composed of two fused rings with opposite polarity, namely, the benzenoid ring (B) and lactone ring (L) with different substitutions in **1–4**. The planar geometry of benzene and lactone ring together (benzolactone ring) supports the observation regarding the aromatic character of coumarin derivatives found in the Cambridge Structural Database³³ reported previously for the benzolactone ring.^{34–43} The geometric parameters of theoretically computed optimized structures of four compounds when compared with the X-ray crystal structures do not show a large difference; the largest deviation in bond distance is 0.03 Å (Table 2). In the X-ray crystal structure of all the compounds, the shortest bond length and the largest angle are observed for C7–C8 and C7–C8–C9, respectively, whereas the other angles

are in the normal range (Table 2). Similar variations in the geometric parameters of the lactone ring (L) of the coumarin skeleton have been reported previously.^{34–43} The bond lengths (Table 2) of the molecular fragment in **1–4** agree well with the mean values of relevant bond distances obtained with MOGUL⁴⁴ from searches based on related molecular fragments run on the CSD.³³ In **4**, the allyloxy group at C(3) is nearly coplanar with the benzenoid ring (B) as indicated by the C(10)–O(3)–C(3)–C(4) torsion angle 3.26(2)°. This coplanarity is comparable with the structures reported earlier with similar substituents.^{39–43} The wide-angle of C(4)–C(3)–O(3) and the narrow-angle of O(3)–C(3)–C(2) show that the allyloxy group is slightly tilted to the C(2) direction.

In the title compounds, the supramolecular aggregations are stabilized by a combination of weak intermolecular C–H···O hydrogen bonds (Table 3) and extensive π ··· π stacking interactions (Table 4). In **1**, the lactone ring carbon atom C8 in the molecule at (*x*, *y*, *z*) acts as a donor to the carbonyl oxygen atom O2 of the partner molecule at (–*x*, –*y*, –*z*) and forms a cyclic hydrogen bonded dimer with R₂²(8) hydrogen bonding synthon (Figure S1, Supporting Information) in Etter's graph notation.⁴⁵ The interconnection of the monomeric units through π ··· π stacking interaction (Table 4) between benzene and lactone rings of the molecules define a well-connected column which forms a supramolecular stacked ribbon in **1** (Figure 2). To optimize the π -stacking interaction, successive molecules flip alternately

Table 3. Relevant Hydrogen Bonding Parameters (\AA , $^\circ$)

	D–H...A	D–H	H...A	D...A	D–H...A	symmetry
compound 1	C8–H8...O2	0.93	2.53	3.445(2)	167	$-x, -y, -z$
compound 2	O3–H3...O1	0.82	2.33	2.738(2)	112	
	O3–H3...O2	0.82	2.15	2.745(2)	129	$-x, 1/2 + y, 3/2 - z$
	C11–H11A...O3	0.96	2.56	3.356(2)	140	$x, -1 + y, z$
	C11–H11B...O2	0.96	2.60	3.553(2)	175	$x, -1/2 - y, 1/2 + z$
compound 3	C7–H7...O3	0.93	2.65	3.573(2)	171	$3/2 - x, 1/2 + y, 3/2 - z$
	C10–H10A...O2	0.96	2.91	3.831(3)	161	$1 - x, -y, 2 - z$
	C11–H11B...O2	0.96	2.60	3.090(3)	112	$1/2 + x, 1/2 - y, -1/2 + z$
compound 4	C2–H2...O3	0.93	2.55	3.483(2)	179	$-x, -y, -z$
	C8–H8...O1	0.93	2.56	3.472(2)	168	$2 - x, -1/2 + y, 1/2 - z$

Table 4. Geometrical Parameters (\AA , $^\circ$) for the π -Stacking Moieties Involved in the $\pi \cdots \pi$ Interactions for the Title Compounds (1–4)^a

rings i–j	Rc ^b	R1v ^c	R2v ^d	α^e	β^f	γ^g	symmetry
compound 1							
Cg(1)...Cg(2)	3.6370(13)	3.5201(7)	3.5157(8)	0.29	14.84	14.56	$-x, -y, 1 - z$
Cg(1)...Cg(2)	3.6121(13)	3.4895(7)	3.4936(8)	0.29	14.72	14.97	$1 - x, -y, 1 - z$
Cg(2)...Cg(2)	3.9316(14)	3.5191(8)	3.5191(8)	0.00	26.48	26.48	$-x, -y, 1 - z$
Cg(2)...Cg(2)	3.8457(14)	3.4906(8)	3.4905(8)	0.00	24.82	24.82	$1 - x, -y, 1 - z$
compound 2							
Cg(1)...Cg(2)	3.4778(13)	3.3270(4)	3.3228(4)	1.62	17.17	16.94	$-x, -y, 2 - z$
Cg(1)...Cg(2)	3.8249(14)	3.5329(4)	3.4923(4)	1.62	24.07	22.53	$1 - x, -y, 2 - z$
Cg(2)...Cg(2)	4.0495(14)	3.3541(4)	3.3541(4)	0.00	34.08	34.08	$-x, -y, 2 - z$
Cg(2)...Cg(2)	3.6391(13)	3.5058(4)	3.5058(4)	0.00	15.56	15.56	$1 - x, -y, 2 - z$
compound 3							
Cg(1)...Cg(1)	4.0778(10)	3.3556(7)	3.3556(7)	4.55	34.63	34.63	$1 - x, y, 3/2 - z$
Cg(1)...Cg(1)	3.9300(11)	3.3365(7)	3.3365(7)	0.00	31.90	31.90	$3/2 - x, 1/2 - y, 2 - z$
Cg(1)...Cg(2)	3.9122(10)	3.3580(7)	3.4592(7)	3.06	27.84	30.87	$1 - x, y, 3/2 - z$
Cg(1)...Cg(2)	3.7015(11)	3.3410(7)	3.3765(7)	1.81	25.49	25.49	$3/2 - x, 1/2 - y, 2 - z$
Cg(2)...Cg(2)	3.5278(11)	3.4339(7)	3.4339(7)	1.00	13.25	13.25	$1 - x, y, 3/2 - z$
compound 4							
Cg(1)...Cg(2)	3.6684(10)	3.3598(6)	3.3535(6)	1.50(7)	23.91	23.67	$1 + x, y, z$

^aCg(1) and Cg(2) are the centroids of the (O1/C5–C9) and (C1–C6) rings, respectively. ^bCentroid distance between ring i and ring j. ^cVertical distance from ring centroid i to ring j. ^dVertical distance from ring centroid j to ring i. ^eDihedral angle between the first ring mean plane and the second ring mean plane of the partner molecule. ^fAngle between centroids of first ring and second ring mean planes. ^gAngle between the centroid of the first ring and the normal to the second ring mean plane of the partner molecule.

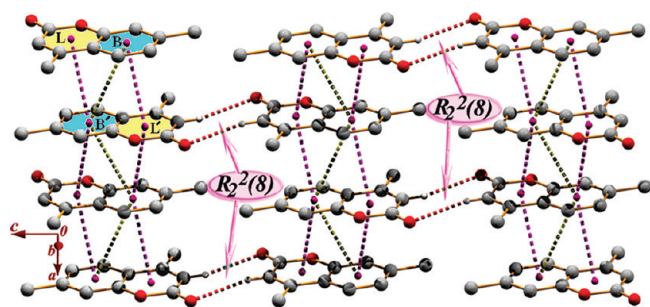


Figure 2. Supramolecular layer in 1 via $\pi \cdots \pi$ stacking and hydrogen bonding interactions. Hydrogen atoms not involve in hydrogen bonding has been omitted for the sake of clarity.

and increase the stability of the ribbon. The benzene ring (B) that is in contact with the lactone ring (L') of the partner molecule has

an intercentroid separation of 3.6370(13) \AA [$-x, -y, 1 - z$]. On the other hand, the intercentroid separation of the lactone ring (L) and benzene ring (B') of the partner molecule is 3.6121(13) \AA [$1 - x, -y, 1 - z$]. The benzene ring (B) is also engaged in π -stacking interaction to the B' ring of the partner molecule and increases the stability of the self-assembly (Figure 2). This π -stacking leads to the molecular aggregation along the (1 0 0) direction. The cooperative π -stacking and hydrogen bonding interaction give rise to the formation of supramolecular layer architecture in 1 (Figure 2).

The molecule 2 has a similar chemical structure as that of 1 except for an additional $-\text{OH}$ group substituted in the benzene ring (B). Despite the close structural similarity between 1 and 2, there are some significant differences in the nature of their spontaneous self-assembly. In 2, the methyl carbon atom C11 in the molecule at (x, y, z) acts as donor to the carbonyl oxygen and hydroxyl oxygen atoms in the molecule at $(x, -1 + y, z)$ and

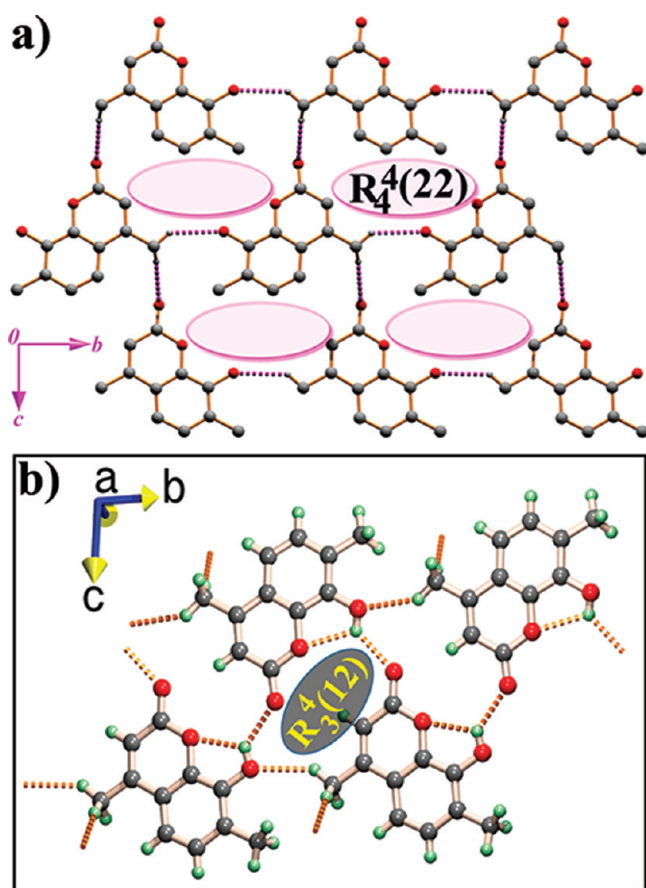


Figure 3. Hydrogen bonded supramolecular ribbon in **2**.

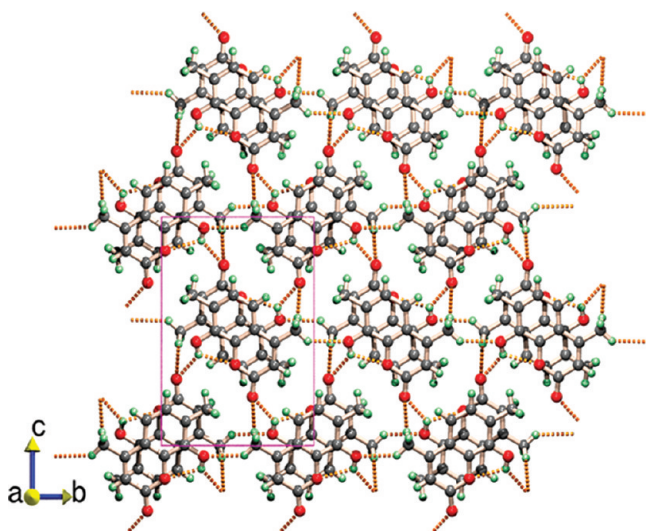


Figure 4. Formation of supramolecular assembly generated through $R_4^4(22)$ and $R_3^4(12)$ ring motif in **2**.

$(x, -1/2 - y, 1/2 + z)$, respectively. These two self-complementary hydrogen bonds result in a supramolecular $R_4^4(22)$ ring motif in **2**. The repetition of these ring motifs generate a 2D supramolecular sheet in $(0\ 1\ 1)$ plane (Figure 3a). Additional hydrogen bonding between the hydroxyl oxygen and lactone carbonyl oxygen results into another cyclic motif. Introduction of

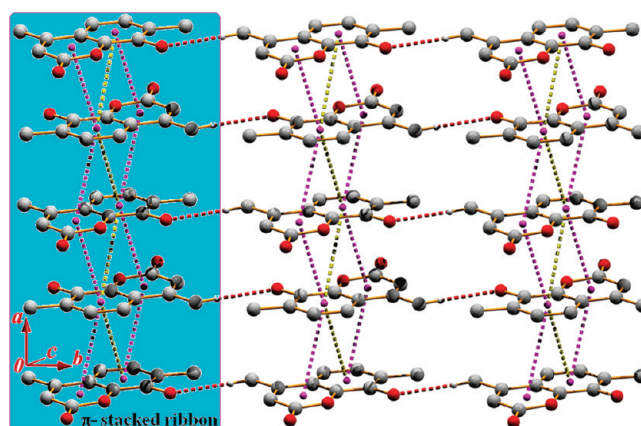


Figure 5. Cooperative dispersive forces and $\pi \cdots \pi$ stacking in **2**.

the $-\text{OH}$ group has disrupted the cyclic hydrogen bonded motif that was observed in **1**. Instead, a $R_3^4(12)$ cyclic hydrogen bonding motif is established here between three adjacent molecules (Figure 3b). The hydrogen bonding parameters are given in Table 3. The molecules are arranged in the $(0\ 1\ 1)$ plane through this hydrogen bonding. The combination of these self-organized superstructures generated through above-mentioned ring motifs leads to aggregation of molecules in the $(0\ 1\ 1)$ plane (Figure 4). Aided by $\pi \cdots \pi$ stacking interactions (Table 4) between the benzene and lactone rings, the molecules organize themselves in well-connected columns (Figure 5).

The lactone ring (L) is in contact with the benzene ring (B) through π -forces which give rise to the formation of the ribbon. Moreover, the benzene rings (B) of the molecule are also in contact with B' ring of the partner molecule via π -stacking interaction. This π -stacking leads to the molecular aggregation along crystallographic a -axis (Figure 5).

On the edges of the stacked ribbon, molecules are recognized, due to their self-complementarity, from layered assembly (Figure 5) through cooperative hydrogen bonding (Table 3) and $\pi \cdots \pi$ forces (Table 4). This dual recognition induced self-assembly of the molecules, where π -forces are responsible for the formation and strengthening of supramolecular layered assembly.

The molecules of **3** are arranged in 202 planes through multiple $\text{C}-\text{H} \cdots \text{O}$ hydrogen bonding (Figure 6) interaction. Two hydrogen bonding motifs exist in the supramolecular assembly, a centrosymmetric motif with four hydrogen bonds is formed by self-complementary association through the wider edge of the molecule, and a cyclic hydrogen bonding motif (motif-A) is established where the oxygen atom of the $-\text{OMe}$ group acts as a hydrogen bond acceptor for the H7 hydrogen atom donated by C7 carbon atom of the lactone ring and the C1 carbon atom donates the H1 proton toward the C10 methyl group. One can also visualize another motif where each molecule interacts with the nearby molecule at their long edges. This gives rise to motif B having four hydrogen bonding contacts. One can expect that motif B will be stronger than motif A.

The molecular planes are stacked over each other due to $\pi \cdots \pi$ interaction (Figure 7). Two types of π -motifs exist in the molecular packing. In one of the π -motifs, the methyl groups of the two molecules are asymmetrically arranged (π -motif A), but in the other it is more symmetrically arranged (π -motif B). The benzene (B) and lactone (L) rings in the molecule at (x, y, z) are in contact with another benzene (B') and lactone (L') rings of

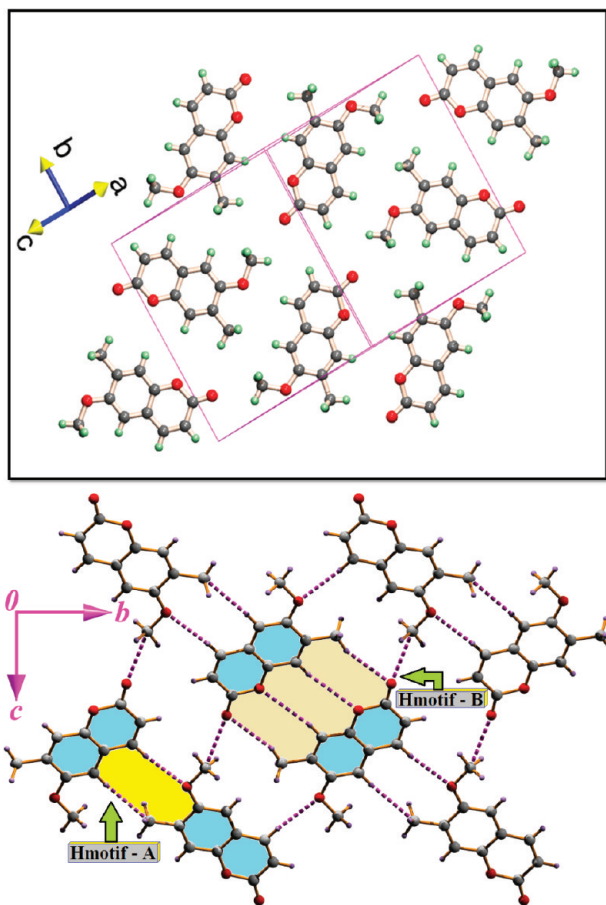


Figure 6. The 2D supramolecular sheet in 3.

the partner molecule at $(1 - x, y, 3/2 - z)$ and generates π -motif A. On the edges of the motif, the lactone ring carbon C7 in the molecule at (x, y, z) acts as donor to the methoxy oxygen in the molecule at $(3/2 - x, 1/2 + y, 3/2 - z)$. The cooperative forces of both hydrogen bonding and π -stacking interactions generate a supramolecular layered assembly in 3 (Figure 7a). In another substructure, the benzene ring and the lactone ring are in contact via π -forces with the neighboring molecule at $(1 - x, y, 3/2 - z)$ and $(3/2 - x, 1/2 - y, 2 - z)$ with intercentroid separations of 3.912(1) Å and 3.702(2) Å respectively to form π -motif B. Here also the methoxy carbon atom acts as donor to the carbonyl oxygen at $(1/2 + x, 1/2 - y, -1/2 + z)$ and the combination of these two types of weak forces results into a supramolecular layered assembly (Figure 7b).

In 4, two coumarin molecules form a cyclic hydrogen bonded dimer with $R_2^2(8)$ hydrogen bonding motif (Figure S2, Supporting Information) in Etter's graph notation.⁴⁵ In this self-complementary hydrogen bond, the allyl oxygen atom acts as acceptor to the H2 proton donated by C2 carbon atom. The hydrogen bonding parameters are given in Table 3. Besides this cyclic motif, a chain of hydrogen bonds with $C_1^1(8)$ motif in Etter's graph notation is responsible for joining of successive dimeric motifs from opposite sides along the b -axis. This leads to a brick-wall architecture of the molecular arrangement in the $(0\ 1\ 1)$ plane (Figure 8). The benzenoid ring B and the lactone ring L interact with the lactone ring L' and the benzenoid ring B' of the partner molecule (prime for partner molecule) through $\pi \cdots \pi$ stacking interaction which forms a supramolecular stacked ribbon in 4, where both molecules

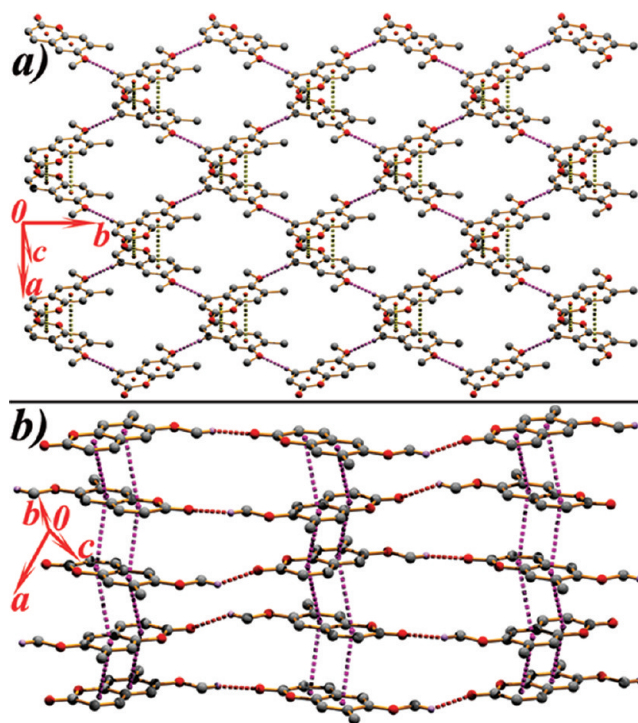


Figure 7. Monomeric units of 3 link one another by self-complementary hydrogen bonding and extensive $\pi \cdots \pi$ interactions leading to the formation of supramolecular layered assembly.

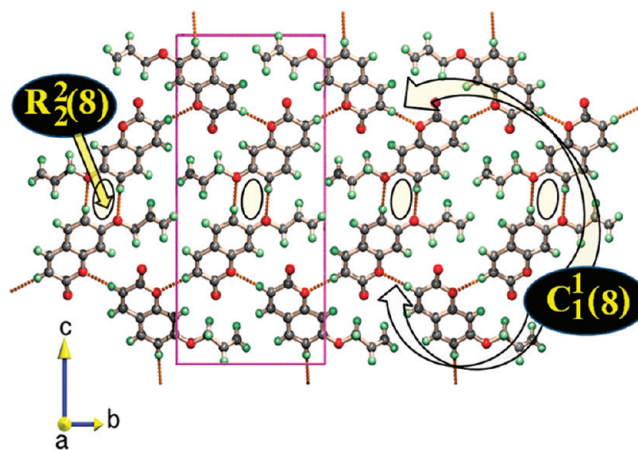


Figure 8. C-H \cdots O hydrogen bonded sheet $(0\ 1\ 1)$ plane in 4.

are related to each other through an inversion center of symmetry. The interconnection between the rings in the molecules at (x, y, z) and $(-1 + x, y, z)$ are parallel, with ring centroid separation of 3.6683(9) Å, forming homodimer and are in agreement with parallel displaced or offset face-to-face π -stacking interactions (Table 4).

An unusual contact between C=O group and the π -system is observed, which is responsible as well for strengthening the molecular assembly. The carbonyl oxygen atom O(2) is in contact with the lactone ring in the molecule at $(1 + x, y, z)$. The distance between O(2) and the centroid of ring L is 3.2804(14) Å [angle C9–O2 \cdots Cg(1) = 89.44(10)°, C9 \cdots Cg(1) = 3.4870(18) Å, where Cg(1) is the centroid of lactone ring]. This gives rise to

the interaction of the lone-pair of O(2) atom with the electron-deficient lactone ring.⁴⁶ These contacts are further supplemented by face-to-face $\pi \cdots \pi$ stacks leading to the formation of supramolecular self-assembly (Figure 9). This dual recognition induced self-assembly of the monomeric units has been observed in the literature.^{10j–n} However, this carbonyl– π interaction has not been thoroughly explored so far as a routine tool in the design and construction of self-assembled structures.

The occurrence of these C=O(l.p.) $\cdots\pi$ contacts produces a unique carbonyl $\cdots\pi/\pi\cdots\pi$ topology to build up molecular architectures. An analysis of the CSD for the lone pair $\cdots\pi$ interaction^{10a} showed a significant carbonyl– π stacking interaction suggested by an angle ω ranging from 0° to 24°, ω being the dihedral angle between C=O and the plane of the aromatic ring. In **4**, the orientation of the carbonyl group is almost parallel to the ring ($\omega \approx 1.5^\circ$). As stated by Egli and Sarkhel,^{10a} this orientation potentially allows hydrogen bonding interactions with the O lone pairs. Moreover, the distance D (corresponding to the distance between the carbonyl oxygen atom and the ring centroid) and the angular distribution [deviation of the angle α (α is the angle C=O \cdots Cg) from 120°] are 3.28 Å and 30.56°, respectively. These values are within the mean values, that is, 3.58 Å and 30.6°,^{10a} on the basis of favorable stacking C=O(l.p.) $\cdots\pi$ interactions found in the CSD. This entire assembly as a whole produces a rare supramolecular lone pair $\cdots\pi/\pi\cdots\pi$ network and illustrates the occurrence of an elegant combination of weak forces in the solid-state structure of **4**.

DFT Results Regarding Hydrogen Bonded and π -Stacked Motifs. In Table 5 we have summarized the theoretical results regarding the hydrogen bonding and π -stacked motifs observed in the X-ray crystal structures of four compounds.

DFT calculation shows a stabilization energy of 25.02 kJ/mol for the hydrogen bonded $R_2^2(8)$ motif of two molecules (Figure S3,

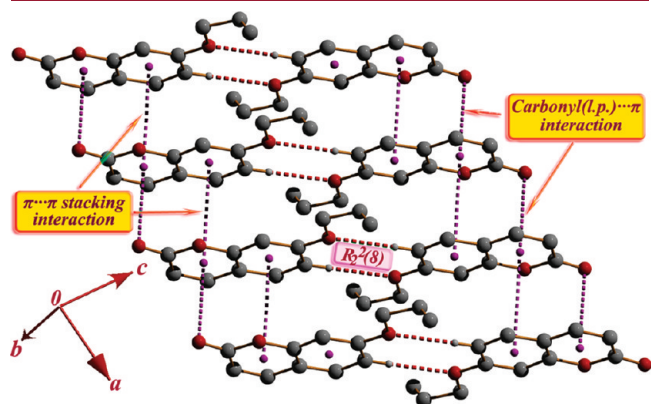


Figure 9. Supramolecular layered-assembly generated through carbonyl (l.p.) $\cdots\pi/\pi\cdots\pi$ interactions in **4**. Hydrogen atoms not involved in hydrogen bonding have been omitted for the sake of clarity.

Supporting Information) in **1**. The molecular electrostatic potential map is depicted in Figure S4, Supporting Information, which shows the concentration of positive and negative charges on the donor and acceptor atoms. DFT calculation shows that the energy of the face to face π -stacked motif of two molecules in **1** is 8.74 kJ/mol (Figure S5, Supporting Information).

DFT calculation shows that the stabilization energy for the $R_3^4(12)$ cyclic hydrogen bonding motif in **2** is 65.40 kJ/mol (Figure S6, Supporting Information) and that of the face-to-face π -stacked motif is 10.67 kJ/mol (Figure S7, Supporting Information).

In compound **3** there are two types of hydrogen bonding and π -stacking motifs. DFT analysis shows a small binding energy of 1.80 kJ/mol (Figure S8, Supporting Information) for the hydrogen bonded motif-A and somewhat larger stabilization energy of 28.16 kJ/mol for motif-B (Figure S9, Supporting Information). Though motif-A has small binding energy the molecular electrostatic potential plot shows the accumulation of the negative charge density on the oxygen atom of the –OMe group and a large positive charge density over the H7 hydrogen atom is responsible for this contact (Figure S10a, Supporting Information). The molecular electrostatic potential plot for motif-B (Figure S10b, Supporting Information) shows that four point contacts are not between the most positive (blue) edge and most negative (red) edges of the molecules, but it is between the same negatively charged wider edges of the partner molecules. The contacts are between relatively less negative to more negative regions on this edge of the molecule. In case of two π -motifs in **3**, methyl groups of the two molecules in one are asymmetrically arranged (π -motif A) and in the other it is more symmetrically arranged (π -motif B). The π -stacking energy of the former motif is 18.16 kJ/mol (Figure S11, Supporting Information) and that of the latter is 19.08 kJ/mol (Figure S12, Supporting Information).

In **4**, the stabilization energy of the cyclic hydrogen bonded dimer with $R_2^2(8)$ motif is 8.91 kJ/mol (Figure S13, Supporting Information). The MEP map of the hydrogen bonded dimer in **4** is displayed in Figure S14, Supporting Information. The energy of the lone pair $\cdots\pi$ stacking motif is 5.15 kJ/mol (Figure S15, Supporting Information).

Hirshfeld Surfaces. The Hirshfeld surfaces of **1–4** are illustrated in Figure 10, showing surfaces that have been mapped over a d_{norm} range of –0.5 to 1.5 Å, shape index (–1.0 to 1.0 Å) and curviness (–4.0 to 0.4 Å). The surfaces are shown as transparent to allow visualization of the benzopyran moiety, in a similar orientation for all the structures, around which they were calculated. The information present in Table 3 is summarized effectively in the spots, with the large circular depressions (deep red) visible on the d_{norm} surfaces indicative of hydrogen bonding contacts and other visible spots are due to H \cdots H contacts. The dominant interactions between hydroxyl O–H and carbonyl O atom in **2** can be seen in Hirshfeld surface plots as the bright red

Table 5. Stabilization Energies of Hydrogen Bonded and π -Stacked Motifs of the Title Compounds **1–4**^a

	1	2	3	4	
hydrogen bonding motifs	25.02 kJ/mol	65.40 kJ/mol	H-motifA 1.80 kJ/mol	H-motifB 28.16 kJ/mol	8.91 kJ/mol
π -stacked motifs	8.74 kJ/mol	10.67 kJ/mol	π -motifA 18.16 kJ/mol	π -motifB 19.08 kJ/mol	5.15 kJ/mol

^a For detailed calculations of energy values see Supporting Information.

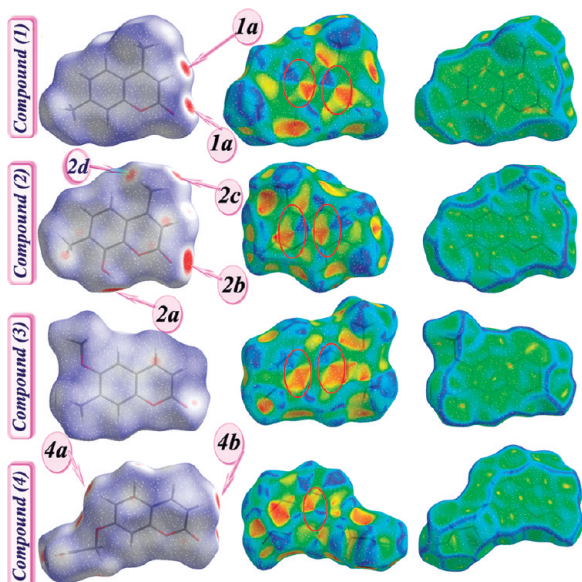


Figure 10. Hirshfeld surfaces mapped with d_{norm} (left), shape index (middle) and curvedness (right) for the title coumarin derivatives 1–4.

area marked as **2b** in Figure 11. The light red spots labeled as **1a**, **2c**, **2d**, and **4a**, **4b** for compounds **1**, **2**, and **4** are due to C–H \cdots O interactions (Figure 10 and Table 3). The small extent of area and light color on the surface indicates weaker and longer contact other than hydrogen bonds.

The O–H \cdots O and C–H \cdots O intermolecular interactions appear as two distinct spikes of almost equal lengths in the 2D fingerprint plots in the region $2.03 \text{ \AA} < (d_e + d_i) < 2.47 \text{ \AA}$ labeled correspondingly as **a**, **b**, etc. Complementary regions are visible in the fingerprint plots where one molecule acts as a donor ($d_e > d_i$) and the other as an acceptor ($d_e < d_i$). The fingerprint plots can be decomposed to highlight particular atom pair close contacts.⁴⁷ This decomposition enables separation of contributions from different interaction types, which overlap in the full fingerprint. The Hirshfeld surface analysis do not show a similar proportion of O \cdots H interactions for each molecules ranging from 14.7% to 18.4%. In all cases, the O \cdots H interactions are represented by a spike in the bottom left (donor) area, whereas the H \cdots O interactions are represented by a spike in the bottom right region in the fingerprint plot and the proportion of H \cdots O interactions has less variety than its O \cdots H counterparts, ranging from 11.6% to 14.0%.

The proportions of O \cdots H/H \cdots O interactions comprising 27.3% of the total Hirshfeld surface for each molecule of **1**. The points in the (d_i , d_e) regions of (1.357 Å, 1.026 Å) in the fingerprint plots are due to C–H \cdots O interactions (Figure 11), representing the lactone ring carbon interacting with carbonyl oxygen, forming a centrosymmetric $R_2^2(8)$ hydrogen bonding motif. In **2**, the O \cdots H/H \cdots O interactions comprise 30.6% of total Hirshfeld surface area. The O \cdots H interactions represented by spike ($d_i = 1.182 \text{ \AA}$, $d_e = 0.851 \text{ \AA}$) represent the hydroxyl oxygen acting as donor to carbonyl oxygen, forming a 1D zigzag chain along the (0 1 0) direction. The H \cdots O interactions represented by spike ($d_i = 0.851 \text{ \AA}$, $d_e = 1.182 \text{ \AA}$) represent the hydroxyl and carbonyl O atoms acting as an acceptor to methyl carbon for the formation of 2D sheet. Compound **3** does not exhibit any classical hydrogen bonds but O \cdots H interaction comprises 32.4% of Hirshfeld surface due to close contacts. In **4**, each molecule comprises

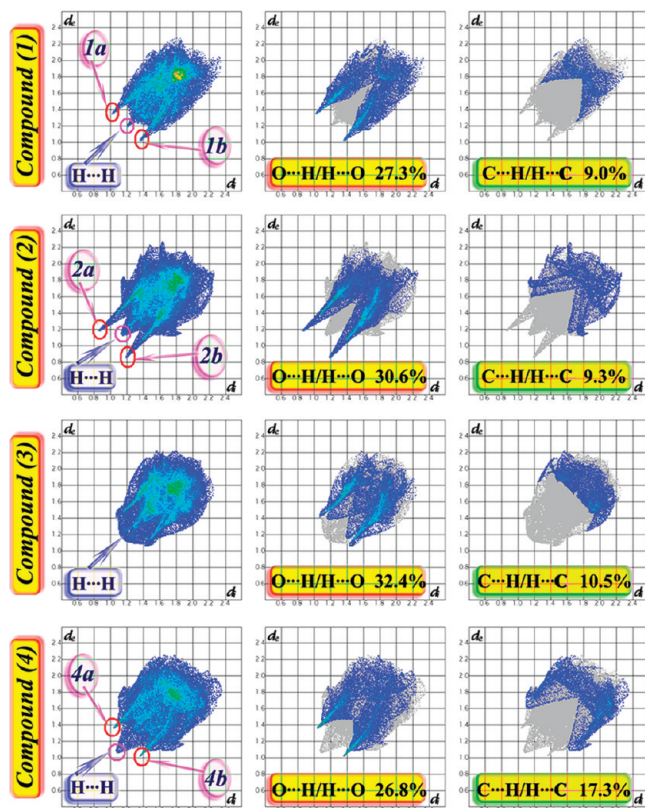


Figure 11. Fingerprint plots of 1–4: Full (left) and resolved into O \cdots H/H \cdots O (middle) and C \cdots H/H \cdots C (right) contacts showing the percentages of contacts contributed to the total Hirshfeld surface area of molecules.

26.8% of total Hirshfeld surface due to O \cdots H/H \cdots O interaction. The spikes in the fingerprint plot represent lactone ring oxygen acting as acceptor to the lactone ring carbon for the formation of 1D chain and the allyl oxygen interacting with the neighboring aryl carbon, forming $R_2^2(8)$ motif. No significant C–H \cdots π interaction has been observed for the substituted coumarin derivatives (1–4), with C–H close contacts varying from 9.0% in **1** to 17.3% in **4**. A significant difference between the molecular interactions in (1–4) in terms of H \cdots H interactions is reflected in the distribution of scattered points in the fingerprint plots, which spread only up to $d_i = d_e = 1.197 \text{ \AA}$ in **1**, $d_i = d_e = 1.132 \text{ \AA}$ in **2**, $d_i = d_e = 1.147 \text{ \AA}$ in **3**, and $d_i = d_e = 1.067 \text{ \AA}$ in **4**.

The relative contributions of the different interactions to the Hirshfeld surfaces were calculated for 1–4 (Figure 12). From the Hirshfeld surfaces, it is clear that the title coumarin derivatives are related to one another where above the plane of the molecule, inspection of the adjacent red and blue triangles on the shape index surface shows that the $\pi\cdots\pi$ stacking interaction is almost identical in the total crystal structures. The presence of $\pi\cdots\pi$ stacking is evident since a flat region toward the bottom of both sides of the molecules and is clearly visible on the curvedness surface. On the d_e surface this feature appears as a relatively flat green region, where the contact distances are all very similar. The corresponding fingerprint plot in Figure 11 shows this interaction as a region of blue/green color on the diagonal at around $d_e \approx d_i \approx 1.78 \text{ \AA}$. The pattern of red and blue triangles on the same region of the shape index surface (Figure 10) is characteristic of $\pi\cdots\pi$ stacking and is used to determine the way in which the

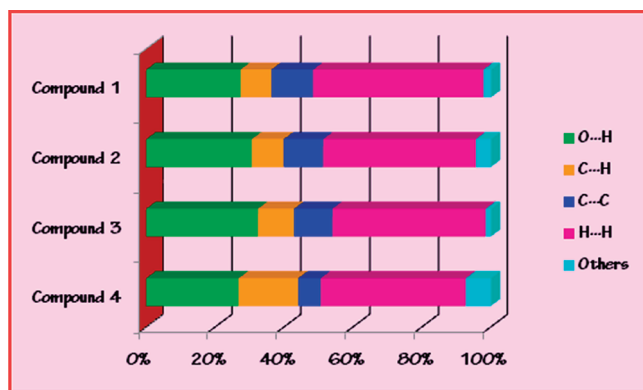


Figure 12. Relative contributions of various intermolecular contacts to the Hirshfeld surface area in 1–4.

molecules overlap and make contact with each other. The pattern of red and blue triangles on this region of both sides of the molecule shows how adjacent molecules in the crystal are related by translation. Blue triangles represent convex regions due to ring carbon atoms of the molecule inside the surface, while red triangles represent concave regions due to carbon atoms of the π stacked molecule above it.

Figure 12 contains the percentages of contributions for a variety of contacts in compounds 1–4. From these values, it can be seen that the $C \cdots C$ contacts, associated with $\pi \cdots \pi$ stacking interactions in the $(d_i, d_e) \approx (1.77 \text{ \AA}, 1.77 \text{ \AA})$ region, are minimal in 4 (only 6.5% of the surface is due to $C \cdots C$ interactions compared with the 11.1%, 11.4%, and 12.1% for 3, 2, and 1, respectively). This quantitatively verifies observations that are obvious from inspecting the different structures. This conclusion is further evident from the shape of the blue outline on the curvedness surface (Figure 10), which unambiguously delineates contacting patches of the molecules. Finally, these examples underline the utility of Hirshfeld surface and in particular, fingerprint plot analysis for the “visual screening” and rapid detection of unusual crystal structures features⁴⁸ through a “whole structure” view of intermolecular interactions.⁴⁹

STRUCTURAL DISCUSSION

Weak noncovalent forces are responsible for organizing organic molecules in the solid state crystalline materials. Except for very few cases, predicting the crystal structure of a given set of organic molecules has remained a difficult task to date. The difficulty lies in our lack of understanding regarding the self-assembly of organic molecules in the presence of multiple noncovalent forces. Understanding of self-assembling behavior of simple organic molecules in the presence of multiple noncovalent forces is the goal of the present study. Coumarin and substituted coumarines being important in many fields, we have chosen a set of four coumarin derivatives in the present study. The basic coumarin framework possesses a benzenoid ring and a lactone ring. It is not difficult to foresee that $\pi \cdots \pi$ stacking interactions will be one of the main forces in governing the packing of these molecules in the solid state, but our aim was to study the effect of hydrogen bonding forces on the molecular packing by arranging various donors and acceptors on the molecular edges of the coumarin molecules. As one can easily see, there are four distinct edges on the rectangular coumarin framework, two long one and two short. The carbonyl O acceptor on the lactone ring is present in

all the molecules at one corner of the rectangular molecular framework. In compounds 1 and 2, the less acidic methyl group is present at the 4 and 7 position. In 2, an addition $-\text{OH}$ substitution is present on the lower edge of the molecule which can possibly act both as donor and acceptor simultaneously because the hydrogen of this group cannot perpendicularly align with respect to the molecular lower edge. The effect of this substitution on the molecular packing is clearly seen by comparing the hydrogen bonding arrangements in 1 and 2. While in 1 a $R_2^2(8)$ hydrogen bonding arrangement leads to dimeric association among the molecules, a distinctly different cyclic $R_3^4(12)$ hydrogen bonding motif is enforced in 2 due to the OH substitution. The hydroxyl group in 2 disrupts the dimeric motif observed in 1 and enforces a $R_3^4(12)$ cyclic motif involving three molecules by simultaneously acting as donor for the carbonyl O atom present on the lactone ring and acceptor for the one of the methyl hydrogens substituted at the 4 position. This motif leads to the ribbon architecture of the self-assembled molecular units in 2. The ribbon propagates along the crystallographic b -axis. Two sets of molecules are positioned symmetrically on both sides of the ribbon, one set running opposite to the other. This arrangement leads to the decoration of the edges of the ribbon by the methyl groups substituted at the 7 position of the molecule. In both 1 and 2, the cooperative π -stacking and hydrogen bonding leads to molecular layers. There is a distinct characteristic of this cooperation. The hydrogen bonding forces act in the molecular plane and π -forces operate perpendicular to the molecular plane. This mode of cooperation of relatively stronger hydrogen bonding forces and comparatively weaker π -stacking forces is a recurring feature observed in the packing of many molecular crystals. The molecular layers observed in 1 is characteristically different from the one observed in 2. In 1, the hydrogen bonded dimers are glued by π -stacking forces leading to a stacked layer of brick wall topology where each dimer is positioned over two other dimers. The methyl groups substituted at 4 and 7 positions decorate the two surfaces of the π -stacked layers. These methyl groups at the molecular corners and other hydrogen atoms at the molecular edges govern the interlayer stacking of the π -stacked layers through dispersive forces. In 2, the stacked molecular ribbons lead to molecular layers with a completely different topology. Each of the ribbons is glued to two adjacent layers on the opposite faces of the molecule at the two edges of the ribbon by π -stacking forces. The topology of the layer is equivalent to that of the equilibrium state of a set of books on a library rack when the support at one end is removed. The uniqueness of this arrangement is in the facilitation of the simultaneous operation of hydrogen bonding forces and π -forces along the same direction. In this slided stacking of hydrogen bonded ribbons not only do π -forces operate but also the methyl group at the 4 position takes part in inter-ribbon hydrogen bonding aiding the π -forces and acts parallel to it. So in 2 the hydrogen bonding forces operate both along the direction of the π -forces and perpendicular to it. Interlayer sacking in this case is governed solely by π -forces.

Interestingly, in 3 where all the substitution is on the benzenoid ring, a methoxy group at the 6 position and the methyl group in the 7 position leads to predominance of π -stacking forces in a direction exactly perpendicular to the plane of the molecule and multipoint $C-\text{H} \cdots \text{O}$ hydrogen bonded contacts in the plane of the molecule at it is four edges. It is very interesting to note that two distinct sets of π -stacking motifs are present in 2. In one type of stacking, the molecular rectangle is parallelly stacked and in the other a L-type stacking arrangement results where two molecular

rectangles are rotated 90° with respect to each other around an a axis passing through the benzenoid rings. Similarly, two sets of hydrogen bonding motifs are present in the molecular plane. In one set, the molecular rectangles are united along their self-complementary long lower edge with four C–H \cdots O contacts. Both the carbonyl O atom and the lactone ring O atom act as acceptor for the methyl hydrogen at the 7-position and the H4 hydrogen of C4 carbon atom on the benzenoid ring. The other hydrogen bonded motif is the result of the long edge to short edge hydrogen bonding association of the rectangular molecule. The O atom of the methoxy group acts as a acceptor for the H7 hydrogen attached to C7 carbon atom on the upper long molecular edge of the molecule. There is an unusual short contact (2.942 Å) between the H1 hydrogen attached to C1 carbon atom on the upper molecular edge and the methyl group at the 7 position. The preliminary DFT calculation also establishes the authenticity of this hydrogen bonded motif having this unusual contact confirming that it is not the artifact of packing effect. A high level calculation is underway to establish the exact nature of the forces associated with this short contact.

In compound **4**, the O atom of the substituted allyloxy group and the lactone ring O atom are responsible for the two types of hydrogen bonding motifs present in the structure. A cyclic $R_2^2(8)$ hydrogen bonding motif leads to molecular dimers. This hydrogen bonding force operates in the molecular plane and joins two rectangular molecules at one of their short edges with the two dangling allylic groups at the opposite end of the long edges. π -stacking forces unite these molecular dimers along a direction perpendicular to the molecular plane that leads to the formation of molecular ribbons. This π -stacking is aided by the carbonyl (lone-pair) $\cdots\pi$ interaction between the carbonyl O atom on the lactone ring and the π -cloud of the lactone ring of the symmetry related molecule. To facilitate this interaction the $\pi\cdots\pi$ interaction is side wise displaced stacking type. Successive molecular ribbons are joined at their short edges due to the formation of $C_2^2(9)$ hydrogen bond chain motif among three successive ribbons. This leads the brick wall architecture of the ribbons in the three-dimensional packing in the crystal. Compound **4** is a rare example where lone-pair $\cdots\pi$ forces cooperate with $\pi\cdots\pi$ and hydrogen bonding forces.

All the molecules of **1–4** are self-associated through π -stacking interactions forming homodimers. Each of the two molecules interacts through parallel displaced $\pi\cdots\pi$ interactions. The intercentroid distances, the dihedral angle between the first ring mean plane and the second ring mean plane of the neighboring molecule, and the angle between the centroid of the first ring and the normal to the second ring mean plane of the partner molecule are in agreement with parallel displaced or offset face-to-face π -stacking interactions. The values of the intercentroid distances between two parallel rings correspond to the sum of the van der Waals radii of two carbon atoms between two benzenoid molecules.⁵⁰ In the title compounds, four π -stacking interactions like B \cdots L', B' \cdots L, B \cdots B', and B' \cdots B are found as common features in the homodimers of **1**, **2**, and **3**, whereas compound **4** exhibits only B \cdots L' and B' \cdots L type π -stacking interactions. An exception is found for the homodimer of **3**, which exhibits L \cdots L' type interactions. These types of interactions forming homodimers are in agreement with the attractive interaction between two rings with opposite polarity, followed by less repulsive interaction between two rings with low electron density and finally the most repulsive interaction between two rings with high electron density.⁵¹

CONCLUSIONS

In summary, in our continuing effort to understand the role of weak forces in the self-assembly of crystalline solid materials we have studied four closely related coumarin based molecules by X-ray structural analysis and DFT calculations. The crystal structure analysis reveals a particular mode of cooperativity of hydrogen bonding forces and $\pi\cdots\pi$ forces. Each molecule is associated in homodimers through parallel displaced π -stacking interactions between complementary rings of the coumarin backbone. Whereas π -forces generally assemble coumarin based molecules perpendicular to the molecular plane, hydrogen bonding forces unite them in the plane of the molecules at their edges. The four edges of the nearly rectangular molecules can be functionalized intelligently and the architecture of the self-assembled hydrogen bonded layer can be tuned accordingly. A $R_2^2(8)$ hydrogen bonded motif operates in the self-assembly among three of the four compounds studied here. A result of the mutual cooperation of hydrogen bonded forces with this motif and the $\pi\cdots\pi$ forces is the appearance of self-assembled molecular ribbons. Widely asymmetric positions of the substituent groups in compound **3** lead to four point contact at the long molecular edges through C–H \cdots O hydrogen bonding and molecular arrangement in a perfect plane. The unique feature of this compound is the appearance of two types of π -motifs due to orientation degrees of freedom of the molecule satisfying the demand of the hydrogen bonding motifs in the molecular plane. The simple coumarin based molecules studied here reveal how finely the various weak forces such as C–H \cdots O forces, $\pi\cdots\pi$ forces, lone-pair $\cdots\pi$ forces, and dispersive forces cooperate with each other in crystal packing. Generally hydrogen bonding forces and $\pi\cdots\pi$ forces operate in mutually perpendicular but cooperative manner and assembly in the molecular plane can be engineered intelligently influencing the out of plane molecular stacking. This methodology has very important promise for further study in the field of photoinduced dimerization, molecular patterning on substrate surfaces, and crystal engineering in general.

Hirshfeld surface is used to visualize the fidelity of computed crystal structures. The nature of the interplay of the title compounds are more easily understood using Hirshfeld surface analyses. The Hirshfeld surface and its fingerprint plots provide information not only about the areas of close contacts but also about more distant contacts and areas where the interactions are weakest. The fingerprint plots certainly allow a much more detailed scrutiny in comparison to similar structures by displaying all the intermolecular interactions within the crystal and are therefore suitable for analyzing the changes in crystal packing due to different substitutions in the coumarin skeleton.

ASSOCIATED CONTENT

S Supporting Information. Four crystallographic files (CIF); Figures S1–S15 illustrating optimized hydrogen bonding, π -stacking motifs and molecular electrostatic potential map of the title compounds. Details of calculations of stabilization energies for different motifs in **1–4** are described here. This material is available free of charge via the Internet at <http://pubs.acs.org>.

AUTHOR INFORMATION

Corresponding Author

*E-mail: mstk@iacs.res.in (T.K.), atishdipankarjana@yahoo.in (A.D.J.).

ACKNOWLEDGMENT

S.K.S. is grateful to the DST-funded National Single Crystal X-ray Diffraction facility at the Department of Inorganic Chemistry, Indian Association for the Cultivation of Science, India, for data collection. The authors are grateful to Amallesh Roy, Department of Organic Chemistry, IACS, Kolkata for his interest, help, and discussions.

REFERENCES

- (1) (a) Desiraju, G. R. *Crystal Engineering: The Design of Organic Solids*; Elsevier, Amsterdam, 1989; (b) Desiraju, G. R. *Angew. Chem., Int. Ed.* **1995**, *34*, 2311–2327.
- (2) (a) Niu, T.; Jacobson, A. J. *Inorg. Chem.* **1999**, *38*, 5346–5350. (b) Klausmeyer, K. K.; Rauchfuss, T. B.; Wilson, S. R. *Angew. Chem., Int. Ed.* **1998**, *37*, 1694–1696. (c) Ibrahim, A. M. A. *Polyhedron* **1999**, *18*, 2711–2721.
- (3) (a) Dimitrakopoulos, C. D.; Malenfant, P. R. L. *Adv. Mater.* **2002**, *14*, 99–117. (b) Forrest, S. R. *Nature* **2004**, *428*, 911–918. (c) Meng, H.; Sun, F.; Goldfinger, M. B.; Gao, F.; Londono, D. J.; Marshal, W. J.; Blackman, G. S.; Dobbs, K. D.; Dalen, E.; Keys, D. E. *J. Am. Chem. Soc.* **2006**, *128*, 9304–9305.
- (4) (a) Mulder, A.; Huskens, J.; Reinhoudt, D. N. *Org. Biomol. Chem.* **2004**, *2*, 3409–3424. (b) Perdigo, L. M. A.; Champness, N. R.; Beton, P. H. *Chem. Commun.* **2006**, 538–540.
- (5) (a) Desiraju, G. R.; Steiner, T. *The Weak Hydrogen Bond in Structural Chemistry and Biology*; Oxford University Press: Oxford, 1999. (b) Jeffrey, G. A.; Saenger, W. *Hydrogen Bonding in Biological Structures*; Springer: Berlin, 1991. (c) Hamilton, W. C.; Ibers, J. A. *Hydrogen Bonding in Solids*; Benjamin: New York, 1968. (d) Scheiner, S. *Hydrogen Bonding: A Theoretical Perspective*; Oxford University Press: Oxford, 1997. (e) Jeffrey, G. A. *An Introduction to Hydrogen Bonding*; Oxford University Press: Oxford, 1997. (f) Steiner, T. *Angew. Chem., Int. Ed.* **2002**, *41*, 48–76. (g) Zhang, Y.; Yang, Z.; Yuan, F.; Gu, H.; Gao, P.; Xu, B. *J. Am. Chem. Soc.* **2004**, *126*, 15028–15029. (h) Noro, S. I.; Akutagawa, T.; Nakamura, T. *Cryst. Growth Des.* **2007**, *7*, 1205–1208.
- (6) (a) Janiak, C. *J. Chem. Soc., Dalton Trans.* **2000**, 3885–3896. (b) Yamauchi, O.; Odani, A.; Hirota, S. *Bull. Chem. Soc. Jpn.* **2001**, *74*, 1525–1545. (c) Packer, M. J.; Dauncey, M. P.; Hunter, C. A. *J. Mol. Biol.* **2000**, *295*, 71–83. (d) Packer, M. J.; Dauncey, M. P.; Hunter, C. A. *J. Mol. Biol.* **2000**, *295*, 85–103. (e) Müller-Dethlefs, K.; Hobza, P. *Chem. Rev.* **2000**, *100*, 143–168. (f) Ghosh, R.; Jana, A. D.; Pal, S.; Mostafa, G.; Fun, H. K.; Ghosh, B. K. *CrystEngComm* **2007**, *9*, 353–357. (g) Schottel, B. L.; Chifotides, H. T.; Shatruck, M.; Chouai, A.; Pérez, L. M.; Bacsa, J.; Dunbar, K. R. *J. Am. Chem. Soc.* **2006**, *128*, 5895–5912. (h) Jana, A. D.; Ghosh, A. K.; Ghoshal, D.; Mostafa, G.; Chaudhuri, N. R. *CrystEngComm* **2007**, *9*, 304–312. (i) Jana, A. D.; Manna, S. C.; Rosair, G. M.; Drew, M. G. B.; Mostafa, G.; Chaudhuri, N. R. *Cryst. Growth Des.* **2007**, *7*, 1365–1372. (j) Hobza, P.; Selzle, H. L.; Schlag, E. W. *Chem. Rev.* **1994**, *94*, 1767–1785. (k) Kim, K. S.; Tarakeshwar, P.; Lee, J. Y. *Chem. Rev.* **2000**, *100*, 4145–4185. (l) Sinnokrot, M. O.; Sherrill, C. D. *J. Phys. Chem. A* **2006**, *110*, 10656–10668. (m) Lee, E. C.; Kim, D.; Jurecka, P.; Tarakeshwar, P.; Hobza, P.; Kim, K. S. *J. Phys. Chem. A* **2007**, *111*, 3446–3457. (n) Pitonak, M.; Neogrady, P.; Rezac, J.; Jurecka, P.; Urban, M.; Hobza, P. *J. Chem. Theory Comput.* **2008**, *4*, 1829–1834. (o) Singh, N. J.; Min, S. K.; Kim, D. Y.; Kim, K. S. *J. Chem. Theory Comput.* **2009**, *5*, 515–529. (p) Mayer, E. A.; Castellano, R. K.; Diederich, F. *Angew. Chem., Int. Ed.* **2003**, *42*, 1210–1250.
- (7) (a) Nishio, M.; Hirota, M.; Umezawa, Y. *The C–H... π Interaction: Evidence, Nature and Consequences*; Wiley-VCH: New York, 1998; (b) Nishio, M. *CrystEngComm* **2004**, *6*, 130–158. (c) Fernandez-Alonso, M. d. C.; Canada, F. J.; Jimenez-Barbero, J.; Cuevas, G. *J. Am. Chem. Soc.* **2005**, *127*, 7379–7386. (d) Braga, D.; Giuffreda, S. L.; Grepioni, F.; Maini, L.; Polito, M. *Coord. Chem. Rev.* **2006**, *250*, 1267–1285. (e) Schneider, H. J. *Angew. Chem., Int. Ed.* **2009**, *48*, 3924–3977.
- (8) (a) Yamada, S.; Uematsu, N.; Yamashita, K. *J. Am. Chem. Soc.* **2007**, *129*, 12100–12101. (b) Yamada, S.; Misono, T.; Suzuki, S. *J. Am. Chem. Soc.* **2004**, *126*, 9862–9872. (c) Kim, D.; Hu, S.; Tarakeshwar, P.; Kim, K. S.; Lisy, J. M. *J. Phys. Chem. A* **2003**, *107*, 1228–1238. (d) Ma, J. C.; Dougherty, D. A. *Chem. Rev.* **1997**, *97*, 1303–1324. (e) Kim, K. S.; Lee, J. Y.; Lee, S. J.; Ha, T. K.; Kim, D. H. *J. Am. Chem. Soc.* **1994**, *116*, 7399–7400.
- (9) (a) Gamez, P.; Mooibroek, T. J.; Teat, S. J.; Reedijk, J. *Acc. Chem. Res.* **2007**, *40*, 435–444. (b) Mascal, M.; Armstrong, A.; Bartberger, M. D. *J. Am. Chem. Soc.* **2002**, *124*, 6274–6276. (c) Alkorta, I.; Rozas, I.; Elguero, J. *J. Am. Chem. Soc.* **2002**, *124*, 8593–8598. (d) Quinonero, D.; Garau, C.; Rotger, C.; Frontera, A.; Ballester, P.; Costa, A.; Deya, P. M. *Angew. Chem., Int. Ed.* **2002**, *41*, 3389–3392.
- (10) (a) Egli, M.; Sarkhel, S. *Acc. Chem. Res.* **2007**, *40*, 197–205. (b) Egli, M.; Gessner, R. V. *Proc. Natl. Acad. Sci. U.S.A.* **1995**, *92*, 180–184. (c) Gautrot, J. E.; Hodge, P.; Cupertinob, D.; Helliwell, M. *New J. Chem.* **2006**, *30*, 1801–1807. (d) Mooibroek, T. J.; Teat, S. J.; Massera, C.; Gamez, P.; Reedijk, J. *Cryst. Growth Des.* **2006**, *6*, 1569–1574. (e) Santos-Contreras, R. J.; Martínez-Martínez, F. J.; García-Báez, E. V.; Padilla-Martínez, I. I.; Peraza, A. L.; Höpfl, H. *Acta Crystallogr. Sect. C* **2007**, *63*, o239–o242. (f) Lu, Z. L.; Gamez, P.; Mutikainen, I.; Turpeinen, U.; Reedijk, J. *Cryst. Growth Des.* **2007**, *7*, 1669–1671. (g) Wan, C. Q.; Chen, X. D.; Mak, T. C. W. *CrystEngComm* **2008**, *10*, 475–478. (h) Biswas, C.; Drew, M. G. B.; Escudero, D.; Frontera, A.; Ghosh, A. *Eur. J. Inorg. Chem.* **2009**, 2238–2246. (i) Kitson, P. J.; Song, Y. F.; Gamez, P.; De Hoog, P.; Long, D. L.; Parenty, A. D. C.; Reedijk, J.; Cronin, L. *Inorg. Chem.* **2008**, *47*, 1883–1885. (j) Mooibroek, T. J.; Gamez, P.; Reedijk, J. *CrystEngComm* **2008**, *10*, 1501–1515. (k) Choudhury, S. R.; Gamez, P.; Robertazzi, A.; Chen, C. Y.; Lee, H. M.; Mukhopadhyay, S. *Cryst. Growth Des.* **2008**, *8*, 3773–3784. (l) Choudhury, S. R.; Dey, B.; Das, S.; Gamez, P.; Robertazzi, A.; Chan, K. T.; Lee, H. M.; Mukhopadhyay, S. *J. Phys. Chem. A* **2009**, *113*, 1623–1627. (m) Seth, S. K.; Dey, B.; Kar, T.; Mukhopadhyay, S. *J. Mol. Struct.* **2010**, *973*, 81–88. (n) Das, A.; Choudhury, S. R.; Dey, B.; Yalamanchili, S. K.; Helliwell, M.; Gamez, P.; Mukhopadhyay, S.; Estarellas, C.; Frontera, A. *J. Phys. Chem. B* **2010**, *114*, 4998–5009. (o) Das, A.; Choudhury, S. R.; Estarellas, C.; Dey, B.; Frontera, A.; Hemming, J.; Helliwell, M.; Gamez, P.; Mukhopadhyay, S. *CrystEngComm* **2011**, *13*, 4519–4527. (p) Seth, S. K.; Saha, I.; Estarellas, C.; Frontera, A.; Kar, T.; Mukhopadhyay, S. *Cryst. Growth Des.* **2011**, *11*, 3250–3265.
- (11) (a) Nyburg, S. C.; Faerman, C. H. *Acta Crystallogr. Sect. B* **1985**, *41*, 274–279. (b) Munakata, M.; Kuroda-Sowa, T.; Maekawa, M.; Hirota, A.; Kitagawa, S. *Inorg. Chem.* **1995**, *34*, 2705–2710. (c) Bond, A. D.; Haynes, D. A.; Pask, C. M.; Rawson, J. M. *J. Chem. Soc., Dalton Trans.* **2002**, 2522–2531. (d) Rovira, C.; Novoa, J. J. *Chem.—Eur. J.* **1999**, *5*, 3689–3697.
- (12) (a) Fujihara, H.; Yabe, M.; Chiu, J. J.; Furukawa, N. *Tetrahedron Lett.* **1991**, *32*, 4345–4348. (b) Shima, H.; Furukawa, N. *Tetrahedron* **1995**, *51*, 12239–12256. (c) Ghosh, A. K.; Ghoshal, D.; Drew, M. G. B.; Mostafa, G.; Chaudhuri, N. R. *Struct. Chem.* **2006**, *17*, 85–90.
- (13) (a) Carlucci, L.; Ciani, G.; Gudenberg, D. W. V.; Proserpio, D. M. *Inorg. Chem.* **1997**, *36*, 3812–3813. (b) Mendizabal, F.; Pyykkö, P. *Phys. Chem. Chem. Phys.* **2004**, *6*, 900–905. (c) Margraf, G.; Bats, J. W.; Bolte, M.; Lerner, H. W.; Wagner, M. *Chem. Commun.* **2003**, 956–957.
- (14) (a) Baures, P. W.; Rush, J. R.; Schroeder, S. D.; Beatty, A. M. *Cryst. Growth Des.* **2002**, *2*, 107–110. (b) Moorthy, J. N.; Venkatesan, K. *J. Mater. Chem.* **1992**, *2*, 675–676.
- (15) (a) Moorthy, J. N.; Mal, P.; Natarajan, R.; Venugopalan, P. *Org. Lett.* **2001**, *3*, 1579–1582. (b) Moorthy, J. N.; Mal, P.; Natarajan, R.; Venugopalan, P. *J. Org. Chem.* **2001**, *66*, 7013–7019. (c) Mal, P.; Lourderaj, U.; Parveen, P.; Venugopalan, J. N.; Moorthy; Sathyamurthy, N. *J. Org. Chem.* **2003**, *68*, 3446–3453. (d) Moorthy, J. N.; Venkatakrishnan, P.; Mal, P.; Venugopalan, P. *J. Org. Chem.* **2003**, *68*, 327–330.
- (16) Gnanaguru, K.; Ramasubbu, N.; Venkatesan, K.; Ramamurthy, V. *J. Org. Chem.* **1985**, *50*, 2337–2346.
- (17) SAINT, Version 6.36a; Bruker-AXS, Inc.: Madison, Wisconsin, USA, 2002.
- (18) Sheldrick, G. M. *SHELXS 97, Program for Structure Solution*, University of Gottingen, Germany, 1997.
- (19) Sheldrick, G. M. *SHELXL97, Program for Crystal Structure Refinement*; University of Gottingen, Germany, 1997.

- (20) Spek, A. L. *PLATON*, Molecular Geometry Program. *J. Appl. Crystallogr.* **2003**, *36*, 7–13.
- (21) Farrugia, L. J. *WinGX-A* Windows Program for Crystal Structure Analysis. *J. Appl. Crystallogr.* **1999**, *32*, 837–838.
- (22) Schmidt, M. W.; Baldridge, K. K.; Boatz, J. A.; Elbert, S. T.; Gordon, M. S.; Jensen, J. H.; Koseki, S.; Matsunaga, N.; Nguyen, K. A.; Su, S. J.; Windus, T. L.; Dupuis, M.; Montgomery Jr., J. A. *PC GAMESS*, version 6.4. *J. Comput. Chem.* **1993**, *14*, 1347–1363.
- (23) Spackman, M. A.; McKinnon, J. J. *CrystEngComm* **2002**, *4*, 378–392.
- (24) (a) McKinnon, J. J.; Jayatilaka, D.; Spackman, M. A. *Chem. Commun.* **2007**, 3814–3816. (b) Spackman, M. A.; McKinnon, J. J.; Jayatilaka, D. *CrystEngComm* **2008**, *10*, 377–388. (c) Spackman, M. A.; Jayatilaka, D. *CrystEngComm* **2009**, *11*, 19–32. (d) Hirshfeld, F. L. *Theor. Chim. Acta* **1977**, *44*, 129–138. (e) Clausen, H. F.; Chevallier, M. S.; Spackman, M. A.; Iversen, B. B. *New. J. Chem.* **2010**, *34*, 193–199. (f) Chattopadhyay, B.; Mukherjee, A. K.; Narendra, N.; Hemantha, H. P.; Sureshbabu, V. V.; Helliwell, M.; Mukherjee, M. *Cryst. Growth Des.* **2010**, *10*, 4476–4484.
- (25) (a) Seth, S. K.; Saha, N. C.; Ghosh, S.; Kar, T. *Chem. Phys. Lett.* **2011**, *506*, 309–314. (b) Seth, S. K.; Sarkar, D.; Kar, T. *CrystEngComm* **2011**, *13*, 4528–4535. (c) Seth, S. K.; Sarkar, D.; Roy, A.; Kar, T. *CrystEngComm* **2011**, DOI: 10.1039/c1ce05670k.
- (26) (a) Spackman, M. A.; Byrom, P. G. *Chem. Phys. Lett.* **1997**, *267*, 215–220. (b) McKinnon, J. J.; Mitchell, A. S.; Spackman, M. A. *Chem.—Eur. J.* **1998**, *4*, 2136–2141.
- (27) McKinnon, J. J.; Spackman, M. A.; Mitchell, A. S. *Acta Crystallogr. Sect. B* **2004**, *60*, 627–668.
- (28) (a) Rohl, A. L.; Moret, M.; Kaminsky, W.; Claborn, K.; McKinnon, J. J.; Kahr, B. *Cryst. Growth Des.* **2008**, *8*, 4517–4525. (b) Parkin, A.; Barr, G.; Dong, W.; Gilmore, C. J.; Jayatilaka, D.; McKinnon, J. J.; Spackman, M. A.; Wilson, C. C. *CrystEngComm* **2007**, *9*, 648–652.
- (29) Wolff, S. K.; Grimwood, D. J.; McKinnon, J. J.; Jayatilaka, D.; Spackman, M. A. *Crystal Explorer 2.0*; University of Western Australia: Perth, Australia, 2007.
- (30) Allen, F. H.; Kennard, O.; Watson, D. G.; Brammer, L.; Orpen, A. G.; Taylor, R. J. *Chem. Soc. Perkin Trans.* **1987**, *2*, S1–S19.
- (31) Koenderink, J. J.; van Doorn, A. J. *Image Vision Comput.* **1992**, *10*, 557–564.
- (32) Farrugia, L. J. *ORTEP III*, Version 1.06; Department of Chemistry, University of Glasgow: Scotland, UK, 1997.
- (33) Allen, F. H. *Acta Crystallogr., Sect. B* **2002**, *58*, 380–388.
- (34) Moorthy, J. N.; Venkatakrishnan, P.; Savitha, G.; Weiss, R. G. *Photochem. Photobiol. Sci.* **2006**, *5*, 903–913.
- (35) Moorthy, J. N.; Venkatakrishnan, P. *Cryst. Growth Des.* **2007**, *7*, 713–718.
- (36) Naveen, S.; Anandalwar, S. M.; Prasad, J. S.; Manvar, D.; Mishra, A.; Acharya, H.; Shah, A. *Anal. Sci.* **2006**, *22*, x173–x174.
- (37) Kurosaki, H.; Sharma, R. K.; Otsuka, M.; Goto, M. *Anal. Sci.* **2003**, *19*, 647–648.
- (38) Kimura, M.; Watson, W. H. *Cryst. Struct. Commun.* **1980**, *9*, 257.
- (39) Ueno, K. *Acta Crystallogr., Sect. C* **1985**, *41*, 1786–1789.
- (40) Ramasubbu, N.; Row, T. N. G.; Ramamurthy, V.; Venkatesan, K.; Rao, C. N. R. *Acta Crystallogr., Sect. A* **1981**, *37*, C86.
- (41) Carlon, R. P.; Jourdain, N.; Reymond, J. L. *Chem.—Eur. J.* **2000**, *6*, 4154–4162.
- (42) Napolitano, H. B.; Silva, M.; Ellena, J.; Rodrigues, B. D. G.; Almeida, A. L. C.; Vieira, P. C.; Oliva, G.; Thiemann, O. H. *Braz. J. Med. Biol. Res.* **2004**, *37*, 1847–1852.
- (43) Gupta, V. K.; Goswami, S.; Gupta, B. D. *Anal. Sci.* **2006**, *22*, x11–x12.
- (44) Bruno, I. J.; Cole, J. C.; Kessler, M.; Luo, J.; Motherwell, W. D. S.; Purkis, L. H.; Smith, B. R.; Taylor, R.; Cooper, R. L.; Harris, S. E.; Orpen, A. G. *J. Chem. Inf. Comput. Sci.* **2004**, *44*, 2133–2144.
- (45) (a) Etter, M. C. *Acc. Chem. Res.* **1990**, *23*, 120–126. (b) Etter, M. C.; MacDonald, J. C.; Bernstein, J. *Acta Crystallogr. Sect. B* **1990**, 256–262.
- (46) Garcia-Baez, E. V.; Martinez-Martinez, F. J.; Hopfl, H.; Padilla-Martinez, I. I. *Cryst. Growth. Des.* **2003**, *3*, 35–45.
- (47) Spackman, M. A.; Byrom, P. G. *Chem. Phys. Lett.* **1997**, *267*, 215–220.
- (48) Fabbiani, F. P. A.; Byrne, L. T.; McKinnon, J. J.; Spackman, M. A. *CrystEngComm* **2007**, *9*, 728–731.
- (49) McKinnon, J. J.; Spackman, M. A.; Mitchell, A. S. *Acta Crystallogr., Sect. B* **2004**, *60*, 627–668.
- (50) (a) Hunter, C. A.; Singh, J.; Thornton, J. M. *J. Mol. Biol.* **1991**, *218*, 837–846. (b) Singh, J.; Thornton, J. M. *J. Mol. Biol.* **1990**, *211*, 595–615.
- (51) Cozzi, F.; Cinquini, M.; Annuziata, R.; Siegel, J. S. *J. Am. Chem. Soc.* **1993**, *115*, 5330–5331.